Nanoscale Research Letters

NANO EXPRESS

Open Access

$NiCo_2S_4$ Nanocrystals on Nitrogen-Doped Carbon Nanotubes as High-Performance Anode for Lithium-Ion Batteries

Haisheng Han[1], Yanli Song[1], Yongguang Zhang[1*], Gulnur Kalimuldina[2] and Zhumabay Bakenov[3]

Abstract

In recent years, the development of lithium-ion batteries (LIBs) with high energy density has become one of the important research directions to fulfill the needs of electric vehicles and smart grid technologies. Nowadays, traditional LIBs have reached their limits in terms of capacity, cycle life, and stability, necessitating their further improvement and development of alternative materials with remarkably enhanced properties. A nitrogen-containing carbon nanotube (N-CNT) host for bimetallic sulfide ($NiCo_2S_4$) is proposed in this study as an anode with attractive electrochemical performance for LIBs. The prepared $NiCo_2S_4$/N-CNT nanocomposite exhibited improved cycling stability, rate performance, and an excellent reversible capacity of 623.0 mAh g^{-1} after 100 cycles at 0.1 A g^{-1} and maintained a high capacity and cycling stability at 0.5 A g^{-1}. The excellent electrochemical performance of the composite can be attributed to the unique porous structure, which can effectively enhance the diffusivity of Li ions while mitigating the volume expansion during the charge–discharge processes.

Keywords: Anode, $NiCo_2S_4$, Nitrogen-doped carbon nanotube, Lithium-ion batteries, Binary metal sulfides

Background

Lithium-ion battery (LIB) is a leading battery technology used in portable electronic devices, electric vehicles, and renewable energy storage [1, 2]. Therefore, the development of LIBs with a high energy density has become a research direction crucial for the sustainable development of various sectors of economics and industry [3–5]. For instance, the specific energy density of a commercial graphite anode material reached its theoretical capacity of 372 mAh g^{-1}, which does not leave much room for its further enhancement to satisfy the performance requirements of emerging electronics and electric vehicle technologies [6, 7]. As a result, it is essential to develop alternative anode materials for LIBs to satisfy the needs of the modern society.

Transition-metal sulfides (TMSs) offer remarkably higher specific capacity than traditional electrode materials [8–12]. Recently, TMSs have been reported as anodes with excellent conductivity and catalytic activity. Among them, binary nickel–cobalt sulfide ($NiCo_2S_4$) exhibits a high theoretical specific capacity (703 mAh g^{-1}), an excellent electronic conductivity (1.26×10^6 S m^{-1}), and a greater abundance of redox reaction sites [13–17]. The reported general charge/discharge mechanism of $NiCo_2S_4$ with lithium (Li) involves the following reactions:

$$NiCo_2S_4 + 8Li^+ + 8e^- \rightarrow Ni + Co + 4Li_2S \quad (1)$$

$$Ni + xLi_2S \leftrightarrow NiS_x + 2xLi^+ + 2xe^- \quad (2)$$

$$Co + xLi_2S \leftrightarrow CoS_x + 2xLi^+ + 2xe^- \quad (3)$$

However, despite the large Li storage capacity of $NiCo_2S_4$, there are still problems related to the low

*Correspondence: yongguangzhang@hebut.edu.cn
[1] School of Materials Science and Engineering, Tianjin Key Laboratory of Materials Laminating Fabrication and Interface Control Technology, Hebei University of Technology, Tianjin 300130, China
Full list of author information is available at the end of the article

reversibility of charge/discharge processes due to the accompanying volume variation, leading to material disintegration and consequently severe capacity fading [18]. Another serious problem originates from the shuttle effect of polysulfides produced by the dissolution of lithium polysulfide (LPS) in the electrolyte, resulting in a low capacity retention as well [19, 20].

To overcome the issues of $NiCo_2S_4$ anodes related to the volume change and LPS dissolution, various approaches including nanostructuring and use of carbonaceous additives and carbon-based hosts have been developed with promising results. Nanostructuring and its combination with carbon/graphene networks can increase the electrode–electrolyte interface contact area and shorten the Li-ion pathways, leading to a higher specific capacity [18]. Therefore, this study reports the in situ growth of $NiCo_2S_4$ nanoparticles onto carbon nanotubes (CNT) structure using a hydrothermal method. Furthermore, to increase the electroactivity of the electrode material, the nitrogen (N) heteroatoms were incorporated into the CNT matrix. Such a processing makes N-CNT more conducive, leading to the uniform growth of $NiCo_2S_4$ and thus improving the crystallinity of $NiCo_2S_4$/N-CNT anode. In this unique structure, CNT forms an elastic matrix that enhances the structural stability, improves the ionic conductivity of the composite, and mitigates the volume variation of $NiCo_2S_4$ particles. The $NiCo_2S_4$/N-CNT material maintains good capacity retention during cycling and significantly restrains the voltage fading. The $NiCo_2S_4$/N-CNT composite anode exhibits an initial discharge capacity of 1412.1 mAh g^{-1} at 0.1 A g^{-1}, and the discharge capacity remains at 623.0 mAh g^{-1} after 100 cycles.

Methods

Synthesis of $NiCo_2S_4$

First, 0.074 g of $Co(AC)_2{\cdot}4H_2O$ and 0.037 g of $Ni(Ac)_2{\cdot}4H_2O$ were dissolved in 40 mL ethanol. The solution was stirred on a water bath at 80 °C for 2 h and at room temperature for another 2 h. Then, 0.078 g of thiourea was added to the mixture, which was further continuously stirred for 20 h before transferring the reaction mixture to a 100 mL autoclave. The hydrothermal reaction was carried out at 170 °C for 3 h. After cooling to room temperature, the product was washed several times with deionized water and freeze-dried under reduced pressure.

Synthesis of $NiCo_2S_4$/N-CNT Nanocomposites

First, 68 mg of mildly oxidized CNT was ultrasonically dispersed in 40 mL of ethanol. Then, 0.074 g of $Co(AC)_2{\cdot}4H_2O$ and 0.037 g of $Ni(Ac)_2{\cdot}4H_2O$ were added, and the mixture was stirred on a water bath at 80 °C for 2 h. Next, 2 mL of $NH_3{\cdot}H_2O$ and 0.078 g of thiourea were added to the solution, and the reaction mixture was stirred for 2 h. The reaction mixture was transferred to a 50-mL autoclave, followed by a hydrothermal reaction at 170 °C for 3 h. The product was cooled to room temperature and centrifuged with deionized water several times and freeze-dried. $NiCo_2S_4$/CNT was synthesized following the same method but without the addition of $NH_3{\cdot}H_2O$.

Characterization of Materials

The crystal structure of the as-synthesized samples was characterized by powder X-ray diffraction (XRD, D8 Discover Bruker). X-ray photoelectron spectrometry (XPS) was performed to analyze the elemental composition of the samples using a K-Alpha 1063 analyzer. The morphology of the samples was studied using a scanning electron microscope (SEM, JSM-7100F, JEOL) and a transmission electron microscope (TEM, JEM-2100F). The specific surface area of the samples was calculated using the Brunauer–Emmett–Teller (BET) method based on the N_2 adsorption–desorption isotherms obtained by using a V-Sorb 2800P. Thermogravimetric analysis (TGA) was carried out in air with a heating rate of 10 °C min^{-1}.

Electrochemical Measurements

The electrochemical performance of $NiCo_2S_4$/N-CNT samples was evaluated in CR 2032 coin-type cells. To prepare the electrode slurry, 70 wt% of $NiCo_2S_4$/N-CNT composite, 15 wt% of carbon black (Super P), and 15 wt% of polyvinylidene fluoride (PVDF) binder were mixed in 1-methyl-2-pyrrolidinone (NMP). The slurry was uniformly spread onto a Cu foil using a doctor blade technique and then dried at 70 °C for 8 h in air. Circular disk electrodes were cut after drying, and the cells were assembled in a high-purity Ar-gas (99.9995%) filled glove box (MBraun). The mass loading of $NiCo_2S_4$/N-CNT in the electrodes was about 2 mg cm^{-2}. Pure Li foils were used as reference and counter electrodes, and microporous polypropylene Celgard 2300 was used as a separator. The electrolyte was 1 mol L^{-1} $LiPF_6$ (Aladdin, CAS number: 21324-40-3) in a mixture of ethylene carbonate (EC, Aladdin, CAS number: 96-49-1) and dimethyl carbonate (DMC, CAS number: 616-38-6) with a volume ratio of 1:1. The galvanostatic charge/discharge measurements were conducted using a multichannel battery testing system (Neware BTS4000) at a potential window of 0.01–3.00 V (vs. Li^+/Li). Cyclic voltammetry (CV) and electrochemical impedance spectroscopy (EIS) were performed using an electrochemical workstation (Princeton, VersaState4).

Results and Discussion

Scheme 1 shows the preparation route of $NiCo_2S_4$/N-CNT composite. Initially, the surface of CNT was pretreated with a solution of Ni^{2+} and Co^{2+}. Then, the N atoms were doped into the CNTs via a hydrothermal reaction at 170 °C, while $NiCo_2S_4$ was grown in situ on the surface of CNTs. The crystal structures of $NiCo_2S_4$, $NiCo_2S_4$/CNT, and $NiCo_2S_4$/N-CNT composites were characterized by XRD (Fig. 1a). The characteristic diffraction peaks of $NiCo_2S_4$ (JCPDS 20-0728) were observed in all the three samples. Moreover, the peaks in $NiCo_2S_4$/N-CNT were more pronounced and sharper than those in $NiCo_2S_4$/CNT [21]. It is believed that N-CNT can be used as active nucleation sites to promote the uniform and dense growth of $NiCo_2S_4$ [22]. Figure 1b shows the BET results for the $NiCo_2S_4$/N-CNT nanocomposites. The specific surface area of $NiCo_2S_4$/N-CNT nanocomposites is 62.67 $m^2\ g^{-1}$. As shown in the TGA analysis data (Fig. 1c), the $NiCo_2S_4$/N-CNT nanocomposite exhibited a weight loss at a temperature range of 400–600 °C, which was caused by the combustion of CNTs. Therefore, the content of $NiCo_2S_4$ in the $NiCo_2S_4$/N-CNT composite was determined as ~ 30 wt%.

The SEM results of the samples are shown in Fig. 2a, b. The as-synthesized $NiCo_2S_4$ nanoparticles appear to be more tightly packed and agglomerated. On the other hand, through the introduction of CNT and N-CNT, the $NiCo_2S_4$ nanoparticles were uniformly distributed and deposited to form $NiCo_2S_4$/CNT composite (Fig. 2c, d) and $NiCo_2S_4$/N-CNT (Fig. 2e, f), respectively. However, the density of $NiCo_2S_4$ nanoparticles on the N-CNT surface in $NiCo_2S_4$/N-CNT was significantly higher than that in the $NiCo_2S_4$/CNT composite. This confirms that the introduction of N atoms in CNTs promotes the denser growth of $NiCo_2S_4$ nanoparticles.

The TEM images in Fig. 3a show that the $NiCo_2S_4$ particles have an average diameter of ~ 5 nm and are uniformly distributed on the surface of N-CNTs. In the high-resolution TEM (HRTEM) image of $NiCo_2S_4$/N-CNT shown in Fig. 3b, the nanoparticles of about 5 nm in diameter exhibit a clear lattice fringe of 0.35 nm, corresponding to the (220) plane of $NiCo_2S_4$. Besides, many crooked graphitic lattice fringes were observed around

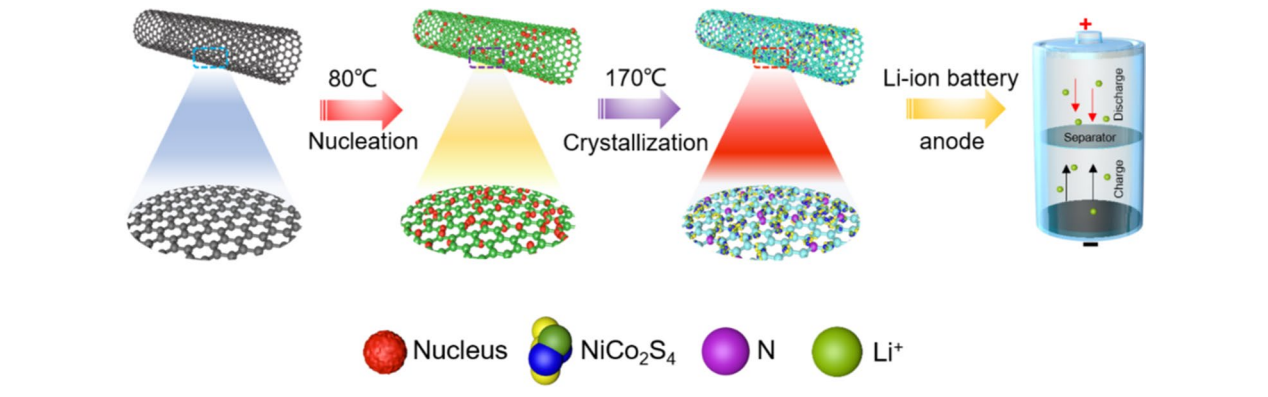

Scheme 1 Schematic representation of $NiCo_2S_4$/N-CNT composite

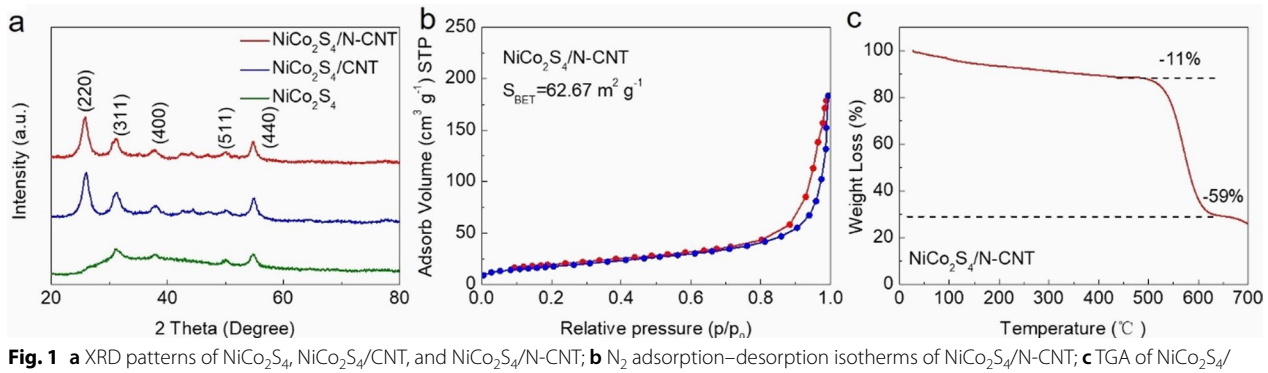

Fig. 1 **a** XRD patterns of $NiCo_2S_4$, $NiCo_2S_4$/CNT, and $NiCo_2S_4$/N-CNT; **b** N_2 adsorption–desorption isotherms of $NiCo_2S_4$/N-CNT; **c** TGA of $NiCo_2S_4$/N-CNT

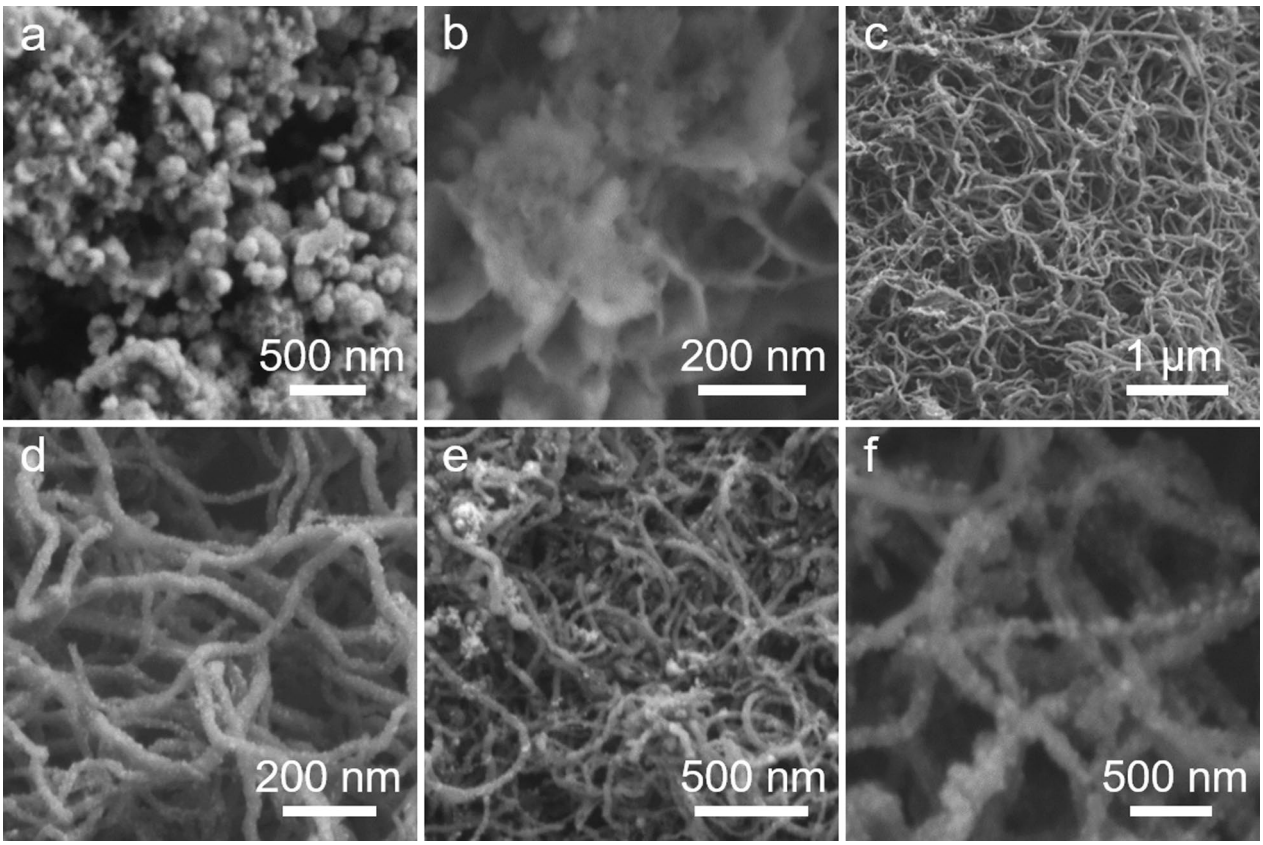

Fig. 2 SEM images of **a**, **b** $NiCo_2S_4$; **c**, **d** $NiCo_2S_4$/CNT; and **e**, **f** $NiCo_2S_4$/N-CNT

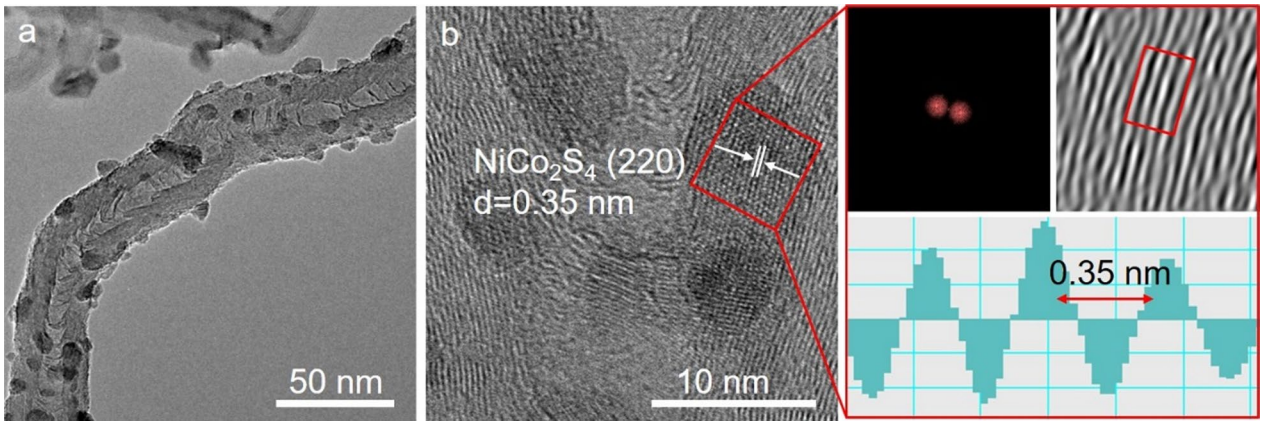

Fig. 3 **a** TEM image; **b** HRTEM image of $NiCo_2S_4$/N-CNT

the nanoparticles. The fast Fourier transform (FFT) and lattice spacing profiles in Fig. 3b further confirmed the incorporation of $NiCo_2S_4$ nanoparticles into the N-CNT structure.

Further, XPS was used to determine the bonding characteristics and surface chemical composition of $NiCo_2S_4$/N-CNT. The Co 2*p* spectra (Fig. 4a) can be divided into two peaks at 778.8 eV and 793.0 eV, corresponding to Co^{3+} and Co^{2+}, respectively [23, 24]. In the N 1*s* spectrum (Fig. 4b), the peaks at 398.3, 399.7, and 400.9 eV can be assigned to the pyridinic, pyrrolic, and graphitic N, respectively [25, 26]. In the XPS spectrum

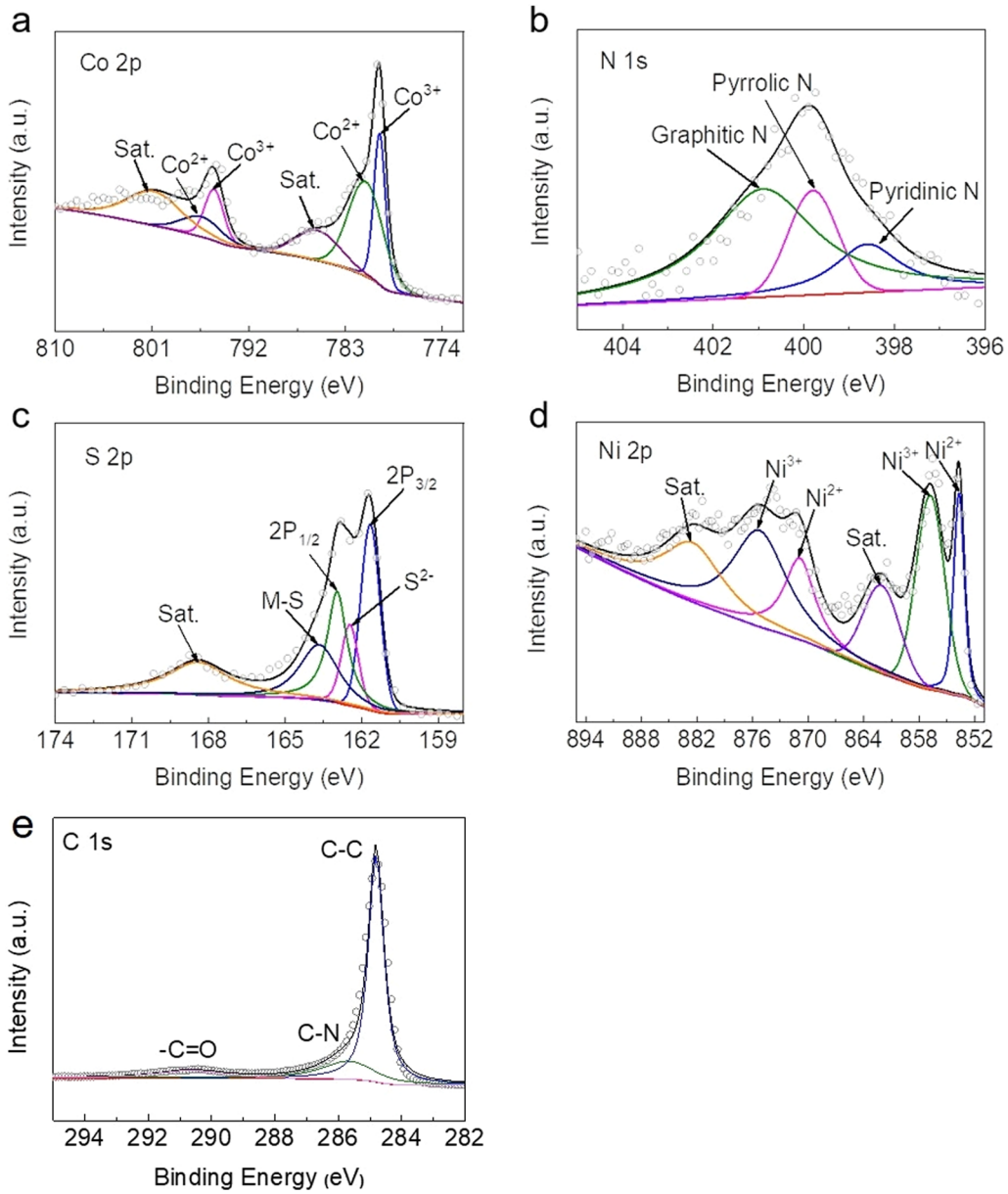

Fig. 4 XPS spectra of **a** Co 2*p*, **b** N 1*s*, **c** S 2*p*, **d** Ni 2*p*, and **e** C 1*s* in $NiCo_2S_4$/N-CNT

of S 2*p* (Fig. 4c), the S $2p_{3/2}$ and S $2p_{1/2}$ can be clearly observed at 161.2 and 163.1 eV, respectively, and the peak at 163.8 eV corresponds to the metal-sulfur bond [27, 28]. As shown in Fig. 4d, in addition to the satellite peaks, the binding energies of Ni 2*p* centered at 854.6 and 856.9 eV correspond to Ni $2p_{3/2}$, and those at 871.1 and 875.5 eV correspond to Ni $2p_{1/2}$. This indicates the presence of both Ni^{3+} and Ni^{2+} in the sample [29, 30]. As shown in Fig. 4e, three fitting peaks are present in the C1s profile at 284.9, 285.7, and 290.4 eV, which can be attributed to C–C, C–N, and –C=O bonds, respectively. In summary, the XPS of $NiCo_2S_4$/N-CNT indicated the formation of a highly ordered crystal structure of $NiCo_2S_4$ and demonstrated the successful introduction of N element into the structure of compounds.

The electrochemical characteristics of $NiCo_2S_4$/N-CNT for Li storage were evaluated by CV and charge–discharge cycling, as shown in Fig. 5 at a potential range of 0.01–3.00 V (vs. Li^+/Li). The cathodic process consisted of three reduction peaks (Fig. 5a) situated at 1.71 V, 1.33 V, and 0.70 V. The strongest peak is positioned at 1.33 V, and two weaker peaks correspond

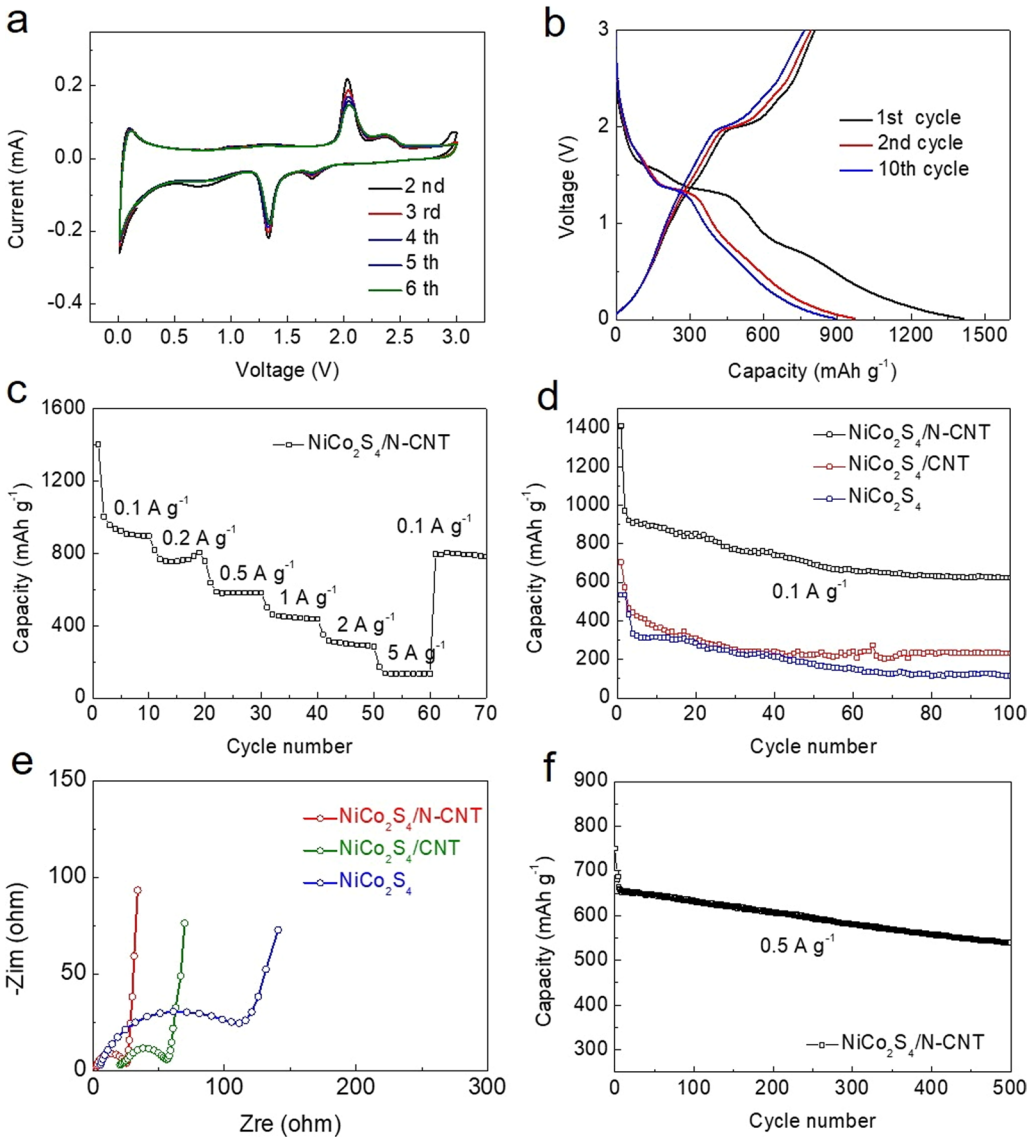

Fig. 5 **a** CVs of $NiCo_2S_4$/N-CNT at a scan rate of 0.1 mV s^{-1} between 0.01 and 3.0 V versus Li^+/Li; **b** charge/discharge curves of $NiCo_2S_4$/N-CNT at 0.1 A g^{-1}; **c** rate capability of $NiCo_2S_4$/N-CNT electrodes at various current rates; **d** cycling performance of $NiCo_2S_4$/N-CNT, $NiCo_2S_4$/CNT, and $NiCo_2S_4$ at 0.1 A g^{-1}; **e** EIS plots of $NiCo_2S_4$/N-CNT, $NiCo_2S_4$/CNT, and $NiCo_2S_4$; **f** cycling performance at a current density of 0.5 A g^{-1}

to the reduction of $NiCo_2S_4$ to Ni and Co. In comparison, the peaks at 1.71 V and 0.70 V correspond to the formation of Li_2S and the SEI film, respectively. In the anodic process, the oxidation peaks at 1.33 V and 2.05 V can be attributed to the oxidation of metallic Co to CoS_x. In addition, there is an intensive peak at 2.32 V resulting from the oxidation reactions of metallic Ni and Co to NiS_x and CoS_x, respectively. The shape of the curve, peak position, and the intensity of peaks are relatively stable in the following cycles, indicating that $NiCo_2S_4$/N-CNT has good stability and reversibility.

Figure 5b shows the charge–discharge curves of $NiCo_2S_4$/N-CNT at 0.1 A g^{-1} for the 1st, 2nd, and 10th cycles. The first charge and discharge capacities of the $NiCo_2S_4$/N-CNT electrode reached 807.6 and 1412.1 mAh g^{-1}, respectively, with the initial coulombic efficiency of 57.2%. The discharge capacities of the 2nd and 10th cycles are 970.7 mAh g^{-1} and 891.1 mAh g^{-1}, respectively. The reversibility of the charge/discharge process improved with the cycle number accompanied with an increased coulombic efficiency. The obtained

CV profiles correspond to the charge/discharge curves of $NiCo_2S_4$/N-CNT.

To further study the electrochemical performance of $NiCo_2S_4$/N-CNT, the rate capability was evaluated at current densities from 0.1 to 5 A g^{-1} (Fig. 5c). The results indicate that the capacity of $NiCo_2S_4$/N-CNT decreased with the increase in current density. When the current density was returned to 0.1 A g^{-1}, the capacity of $NiCo_2S_4$/N-CNT returned to a value of 796.1 mAh g^{-1}, exhibiting about 84% capacity retention and demonstrating that $NiCo_2S_4$/N-CNT exhibits an excellent rate performance. The cycling performance data of $NiCo_2S_4$/N-CNT, $NiCo_2S_4$/CNT, and $NiCo_2S_4$ for 100 cycles at 0.1 A g^{-1} are shown in Fig. 5d. For the initial 50 cycles, the anode undergoes a slight capacity fading. Then, $NiCo_2S_4$/N-CNT anode stabilized its capacity for the rest of the cycles and demonstrated a value of 623.0 mAh g^{-1} after 100 cycles. These results show that compared with the $NiCo_2S_4$/CNT and $NiCo_2S_4$ electrodes, the $NiCo_2S_4$/N-CNT electrode exhibited a remarkably higher discharge specific capacity and better cycle stability. Figure 5e shows the EIS data. The high-frequency semicircles in the Nyquist plots correspond to the charge transfer resistance (R_{ct}) of the electrodes. The $NiCo_2S_4$/N-CNT electrode clearly exhibits the lowest R_{ct} values, suggesting a remarkably enhanced charge/mass transfer kinetics. Figure 5f shows the cycling performance of $NiCo_2S_4$/N-CNT electrode at 0.5 A g^{-1} over 500 cycles. The $NiCo_2S_4$/N-CNT electrode delivers an initial specific discharge capacity of 750.2 mAh g^{-1} and maintains a reversible capacity of 539.3 mAh g^{-1} after 500 cycles, further confirming an excellent cycling and rate capability of this high capacity anode for lithium batteries.

Conclusions

In summary, a $NiCo_2S_4$/N-CNT composite was prepared using a one-pot facile hydrothermal synthesis route. By introducing the N atoms into the CNT structure, uniformly distributed $NiCo_2S_4$ nanoparticles with reduced particle sizes were obtained. The assembled cells with the $NiCo_2S_4$/N-CNT anode demonstrated a high specific capacity of about 623.0 mAh g^{-1} and excellent cycling stability at 0.1 A g^{-1} after 100 cycles. Furthermore, this electrode exhibited an excellent cycling property at 0.5 A g^{-1} over 500 cycles, confirming its ability to maintain its high performance at elevated current densities. Our study shows that this synthesis method is a feasible way to grow $NiCo_2S_4$ nanoparticles with uniform distribution on the surface of a CNT substrate as a high-performance anode for LIBs.

Abbreviations

LIBs: Lithium-ion batteries; CNT: Carbon nanotube; $NiCo_2S_4$: Binary nickel–cobalt sulfide; PVDF: Polyvinylidene fluoride; NMP: *N*-Methyl-2-pyrrolidone; XRD: X-ray powder diffraction; SEM: Scanning electron microscopy; CV: Cyclic voltammetry; EIS: Electrochemical impedance spectroscopy; N-CNT: Nitrogen-containing carbon nanotube; TMS: Transition metal sulfides; LPS: Lithium polysulfide; XPS: X-ray photoelectron spectrometry; TEM: Transmission electron microscope; HRTEM: High-resolution transmission electron microscope; BET: Brunauer–Emmett–Teller; TGA: Thermogravimetric analysis; EC: Ethylene carbonate; DMC: Dimethyl carbonate; FFT: Fast Fourier transform; N: Nitrogen; Li: Lithium.

Authors' contributions

HH and YS contributed to formal analysis ; HH and YS contributed to investigation ; HH contributed to writing–original draft preparation; GK, ZB, and YZ contributed to writing–review and editing ; YZ supervised the study ; YZ contributed to project administration. All authors read and approved the final manuscript.

Funding

This research was funded by Natural Science Foundation of Hebei Province of China (B2020202052); the Program for the Outstanding Young Talents of Hebei Province, China; Chunhui Project of Ministry of Education of the People's Republic of China (Grant No. Z2017010); the Faculty Development Competitive Research Grant Program Grant 110119FD4504 and Collaborative Research Program Grant 091019CRP2114 from Nazarbayev University.

Availability of Data and Materials

All data generated or analyzed during this study are included in this published article.

Declaration

Competing interests

The authors declare that they have no competing interests.

Author details

[1]School of Materials Science and Engineering, Tianjin Key Laboratory of Materials Laminating Fabrication and Interface Control Technology, Hebei University of Technology, Tianjin 300130, China. [2]Department of Mechanical and Aerospace Engineering, Nazarbayev University, Nur-Sultan 010000, Kazakhstan. [3]Department of Chemical and Materials Engineering, National Laboratory Astana, Nazarbayev University, Nur-Sultan 010000, Kazakhstan.

Received: 22 February 2021 Accepted: 3 June 2021
Published online: 12 June 2021

References

1. Ma Y, Liu P, Xie Q, Zhang C, Wang L, Peng D (2020) Intrinsic performance regulation in hierarchically porous Co_3O_4 microrods towards high-rate lithium ion battery anode. Mater Today Energy 16:100383
2. Xu G, Li J, Huang L, Lin W, Sun S (2013) Synthesis of Co_3O_4 nano-octahedra enclosed by facets and their excellent lithium storage properties as anode material of lithium ion batteries. Nano Energy 2:394–402
3. Su Q, Zhang J, Wu Y, Du G (2014) Revealing the electrochemical conversion mechanism of porous Co_3O_4 nanoplates in lithium ion battery by in situ transmission electron microscopy. Nano Energy 9:264–272
4. Zhang C, Song Y, Xu L, Yin F (2020) In situ encapsulation of Co/Co_3O_4 nanoparticles in nitrogen-doped hierarchically ordered porous carbon as high performance anode for lithium-ion batteries. Chem Eng J 380:122545
5. Wang B, Lu X, Tsang C, Wang Y, Au W, Guo H, Tang Y (2018) Charge-driven self-assembly synthesis of straw-sheaf-like Co_3O_4 with superior cyclability and rate capability for lithium-ion batteries. Chem Eng J 338:278–286
6. Lou X, Deng D, Lee J, Feng J, Archer L (2008) Self-supported formation of needlelike Co_3O_4 nanotubes and their application as lithium-ion battery electrodes. Adv Mater 20:258–262
7. Mao Y, Shen X, Wu Z, Zhu L, Liao G (2020) Preparation of Co_3O_4 hollow microspheres by recycling spent lithium-ion batteries and

their application in electrochemical supercapacitors. J Alloy Compd 816:152604
8. Chu K, Li Z, Xu S, Yao G, Xu Y, Niu P, Zheng F (2020) MOF-derived hollow $NiCo_2O_4$ nanowires as stable Li-ion battery anodes. Dalton T 49:10808–10815
9. Liu Y, Han D, Wang L, Li G, Liu S, Gao X (2019) $NiCo_2O_4$ nanofibers as carbon-free sulfur immobilizer to fabricate sulfur-based composite with high volumetric capacity for lithium-sulfur battery. Adv Energy Mater 9:1803477
10. Ding Y, Zeng PY, Fang Z (2020) Spindle-shaped FeS_2 enwrapped with N/S Co-doped carbon for high-rate sodium storage. J Power Sources 450:227688
11. Zeng P, Li J, Ye M, Zhuo K, Fang Z (2017) In situ formation of Co_9S_8/N-C hollow nanospheres by pyrolysisand sulfurization of ZIF-67 for high-performance lithium-ion batteries. Chem Eur J 23:9517–9524
12. Liu Y, Jiang W, Liu M, Zhang L, Qiang C, Fang Z (2019) Ultrafine $Co_{1-x}S$ attached to porous interconnected carbon skeleton for sodium-ion batteries. Langmuir 35:16487–16495
13. Liang H, Wang Z, Guo H, Li X (2017) Unique porous yolk-shell structured Co_3O_4 anode for high performance lithium ion batteries. Ceram Int 43:11058–11064
14. Shin H, Lee W (2018) Ultrathin mesoporous shell Co_3O_4 hollow spheres as high-performance electrode materials for lithium-ion batteries. Mater Chem Phys 214:165–171
15. Zhang X, Yang Z, Li C, Xie A, Shen Y (2017) A novel porous tubular Co_3O_4: Self-assembly and excellent electrochemical performance as anode for lithium-ion batteries. Appl Surf Sci 403:294–301
16. Min F, Ran Y, Min Z, Teng F, Wang S, Wu H, Feng C (2018) Synthesis and electrochemical performance of $NiCo_2S_4$ as anode for lithium-ion batteries. J Nanosci Nanotechno 18:5749–5755
17. Lin Z, Min Z, Chen W, Min F, Wu H, Wang S, Feng C, Zhang Y (2019) $NiCo_2S_4$/carbon nanotube composites as anode material for lithium-ion batteries. J Electron Mater 48:8138–8148
18. Chen H, Ma X, Shen PK (2019) $NiCo_2S_4$ nanocores in-situ encapsulated in graphene sheets as anode materials for lithium-ion batteries. Chem Eng J 364:167–176
19. Wu S, Xia T, Wang J, Lu F, Xu C, Zhang X, Huo L, Zhao H (2017) Ultrathin mesoporous Co3O4 nanosheets-constructed hierarchical clusters as high rate capability and long life anode materials for lithium-ion batteries. Appl Surf Sci 406:46–55
20. Wang X, Zhou B, Guo J, Zhang W, Guo X (2016) Selective crystal facets exposing of dumbbell-like Co_3O_4 towards high performances anode materials in lithium-ion batteries. Mater Res Bull 83:414–422
21. Jain A, Paul B, Kim S, Jain V, Kim J, Rai A (2019) Two-dimensional porous nanodisks of $NiCo_2O_4$ as anode material for high-performance rechargeable lithium-ion battery. J Alloy Compd 772:72–79
22. Zhu F, Xia H, Feng T (2015) Nanowire interwoven $NiCo_2S_4$ nanowall arrays as promising anodes for lithium ion batteries. Mater Technol 30:A53–A57
23. Xia Y, Wang H (2015) $NiCo_2O_4$ polyhedra with controllable particle size as high-performance anode for lithium-ion battery. Ionics 22:159–166
24. Wang J, Wu J, Wu Z, Han L, Huang T, Xin H, Wang D (2017) High-rate and long-life lithium-ion battery performance of hierarchically hollow-structured $NiCo_2O_4$/CNT nanocomposite. Electrochim Acta 244:8–15
25. Zhao F, Zhao X, Peng B, Gan F, Yao M, Tan W, Dong J, Zhang Q (2018) Polyimide-derived carbon nanofiber membranes as anodes for high-performance flexible lithium ion batteries. Chinese Chem Lett 29:1692–1697
26. Wang J, Fan H, Shen Y, Li C, Wang G (2019) Large-scale template-free synthesis of nitrogen-doped 3D carbon frameworks as low-cost ultra-long-life anodes for lithium-ion batteries. Chem Eng J 357:376–383
27. Jin R, Liu G, Liu C, Sun L (2016) High electrochemical performances of hierarchical hydrangea macrophylla like $NiCo_2O_4$ and $NiCo_2S_4$ as anode materials for Li-ion batteries. Mater Res Bull 80:309–315
28. Raj S, Dong Y, Kar P, Mai L, Jin S, Roy P (2018) Hybrid $NiCo_2O_4$-$NiCo_2S_4$ nanoflakes as high-performance anode materials for lithium-ion batteries. ChemistrySelect 3:2315–2320
29. Wang M, Lai Y, Fang J, Qin F, Zhang Z, Li J, Zhang K (2016) Hydrangea-like $NiCo_2S_4$ hollow microspheres as an advanced bifunctional electrocatalyst for aqueous metal/air batteries. Catal Sci Technol 6:434–437
30. Chen J, Jiang J, Liu S, Ren J, Lou Y (2019) MOF-derived bimetal oxides NiO/$NiCo_2O_4$ with different morphologies as anodes for high-performance lithium-ion battery. Ionics 25:5787–5797

Publisher's Note